Gas confinement in compartmentalized coordination polymers for highly selective sorption

Mónica Giménez-Marqués,[1] Néstor Calvo Galve,[1] Miguel Palomino,[2] Susana Valencia,[2] Fernando Rey,[2] Germán Sastre,[2] Iñigo J. Vitórica-Yrezábal,[3] Mónica Jiménez-Ruiz,[4] J. Alberto Rodríguez-Velamazán,[4,5] Miguel A. González,[4] José L. Jordá,[2] Eugenio Coronado,[1] Guillermo Mínguez Espallargas[1]*.

[1] *Instituto de Ciencia Molecular (ICMol), Universidad de Valencia, c/ Catedrático José Beltrán, 2, 46980 Paterna, Spain.*

[2] *Instituto de Tecnología Química (UPV-CSIC), Universidad Politécnica de Valencia – Consejo Superior de Investigaciones Científicas, Av. de los Naranjos s/n, 46022 Valencia, Spain*

[3] *School of Chemistry, University of Manchester, Oxford Road, Manchester, M13 9PL, UK*

[4] *Institut Laue-Langevin, 38042 Grenoble Cedex 9, France*

[5] *Instituto de Ciencia de Materiales de Aragón (ICMA), CSIC – Universidad de Zaragoza, 50009 Zaragoza, Spain*

ABSTRACT

Discrimination between different gases is an essential aspect for industrial and environmental applications involving sensing and separation. Several classes of porous materials have been used in this context, including zeolites and more recently MOFs. However, to reach high selectivities for the separation of gas mixtures is a challenging task that often requires the understanding of the specific interactions established between the porous framework and the gases. Here we propose an approach to obtain an enhanced selectivity based on the use of compartmentalized coordination polymers, named **CCP-1** and **CCP-2**, which are crystalline materials comprising isolated discrete cavities. These compartmentalized materials are excellent candidates for the selective separation of CO_2 from methane and nitrogen. A complete understanding of the sorption process is accomplished with the use of complementary experimental techniques including X-ray diffraction, adsorption studies, inelastic- and quasi-elastic neutron scattering, magnetic measurements and molecular dynamics calculations.

INTRODUCTION

Efficient separation of many light gases (H_2, N_2, O_2, CO, NO, CO_2, CH_4, and many others) is becoming increasingly important from energetic, biological, and environmental standpoints, as is also the effective capture of harmful gases such as H_2S, SO_2, Cl_2, CNCl, NH_3, NO_x, CO, C_2H_2, which are typical components of waste gases from industrial processes.[1] Particularly relevant processes of separation of mixtures of light gases include CO_2/N_2 from exhaust emissions from power plants (important to mitigate the growing level of atmospheric CO_2), acetylene/ethylene (both essential reagents for a range of chemical products and materials), ethylene/ethane (one of the most important separation processes in the petrochemical industry), CO/H_2 (for fuel cells) or CO_2/CH_4 (major components of biogas and natural gas), among others.

Gas sorption by zeolites and MOFs with high surface area and large permanent porosity is well established,[2] and therefore they have successfully been applied for gas separation processes.[3,4] For example they have been postulated as alternatives for amine systems that are traditionally used for CO_2 removal.[5] Even more attractive are porous materials possessing restricted guest-accessible pores in which permanent cavities are inter-connected by small apertures in a long-range order, since they often provide improved selective separations.[6,7] A different approach consists on the use of interpenetrated frameworks, which also result as an effective solution for enhancing selectivity despite the decrease in porosity.[8,9] Typically, these materials are capable of discriminating between different guests based on their size, and even subtle changes in the pore diameter can modify the selectivity.[10] However, the minor difference in sizes of many gases demands other approaches towards enhancing the selectivity, for instance by exploitation of electronic properties such as the quadrupole moment and polarizability. These include ligand functionalization[11,12] and insertion of cations,[13,14] although the strategy that is currently attracting more efforts to enhance the gas separation performance of MOFs consists on tuning the binding interaction of the framework and the gas molecule.[15-22] Thus, introducing specific sites for hard binding of the gas molecules, including generation of exposed metal sites within the framework[15-18] and functionalization of the pores with Lewis basic sites,[19-20] has been shown to increment the interaction of specific molecules such as CO_2 and hydrocarbons. However, a high-energy cost is then required for the regeneration of the material. This energy penalty has been recently overcome by using supramolecular interactions that can be exploited for selective sorption through the soft binding of gases, thus implying a lower energy.[21,22]

Herein we present a conceptually different approach for selective separation of diverse mixtures of gases with the development of unconventional crystalline solids with periodically-organized discrete compartments for gas confinement, capable of interacting with gas molecules despite the absence of large channels or permanent pores. Materials capable of absorbing and orienting guest molecules through the use of networked cages have been recently developed as a new strategy for the determination of molecular structures otherwise unachievable.[23] We combine the concept of networked cages with the presence of latent porosity[24] to achieve a material that selectively separates different mixtures of gases, exploiting both thermodynamic equilibrium and kinetic trapping in the same material. Moreover, this chemical design enhances the interplay between the guests and the frameworks, as we have previously shown, demonstrating that a specific physical property of the framework, in particular spin-crossover phenomena,[25] can be successfully modified through the incorporation of CO_2 molecules.[26,27] We provide now a deep understanding of the gas-framework interactions that has been achieved through combination of X-ray diffraction, inelastic neutron scattering and magnetic measurements, which have been exploited not only to detect but also to evaluate the strength of the adsorption. Additionally, a sorption mechanism has been proposed based on quasi-elastic neutron scattering data and molecular dynamics calculations. This multi-technique detailed analysis, complemented by experimental adsorption data, has provided a clear assessment of the gas sorption process in compartmentalized crystalline solids, thus providing essential information for the development of these solids.

RESULTS AND DISCUSSION

Crystal structure and characterization. The direct combination of the ligand btzx [btzx = bistetrazol-*p*-xylene] with an excess of $Fe(ClO_4)_2 \cdot xH_2O$ or $Fe(BF_4)_2 \cdot 6H_2O$ produces well-defined hexagonal crystals (edge length of *ca.* 2 μm and a thickness of *ca.* 500 nm) of $[Fe(btzx)_3](ClO_4)_2$ (**CCP-1**)[26] and $[Fe(btzx)_3](BF_4)_2$ (**CCP-2**), respectively (CCP stands for Compartmentalized Coordination Polymer). Both isostructural compounds crystallize in the $P6_3/m$ space group and are composed of $[Fe(btzx)_3]^{2+}$ units that form regular cationic chains that run parallel to the crystallographic *c*-axis (Figure 1). The *syn* conformation of the btzx ligands that connect neighboring Fe^{II} yield internal cavities with void volumes of 11.8 % (**CCP-1**) and 12.4 % (**CCP-2**) of the unit cell (discrete voids of 132 $Å^3$ and 140 $Å^3$, respectively), which contain no solvent molecules, as demonstrated by thermogravimetric (TGA) and SQUEEZE analyses.[28] These voids present three rectangular pore windows with dimensions of 6.6 x 6.2 $Å^2$, albeit close inspection of the crystal structure reveals the presence of a window-to-arene arrangement with three adjacent chains resulting in their blockage (see Figure 1). Therefore, this arrangement causes the absence of

permanent channels in solids **CCP-1** and **CCP-2**, which can thus be best described as compartmentalized coordination polymers.

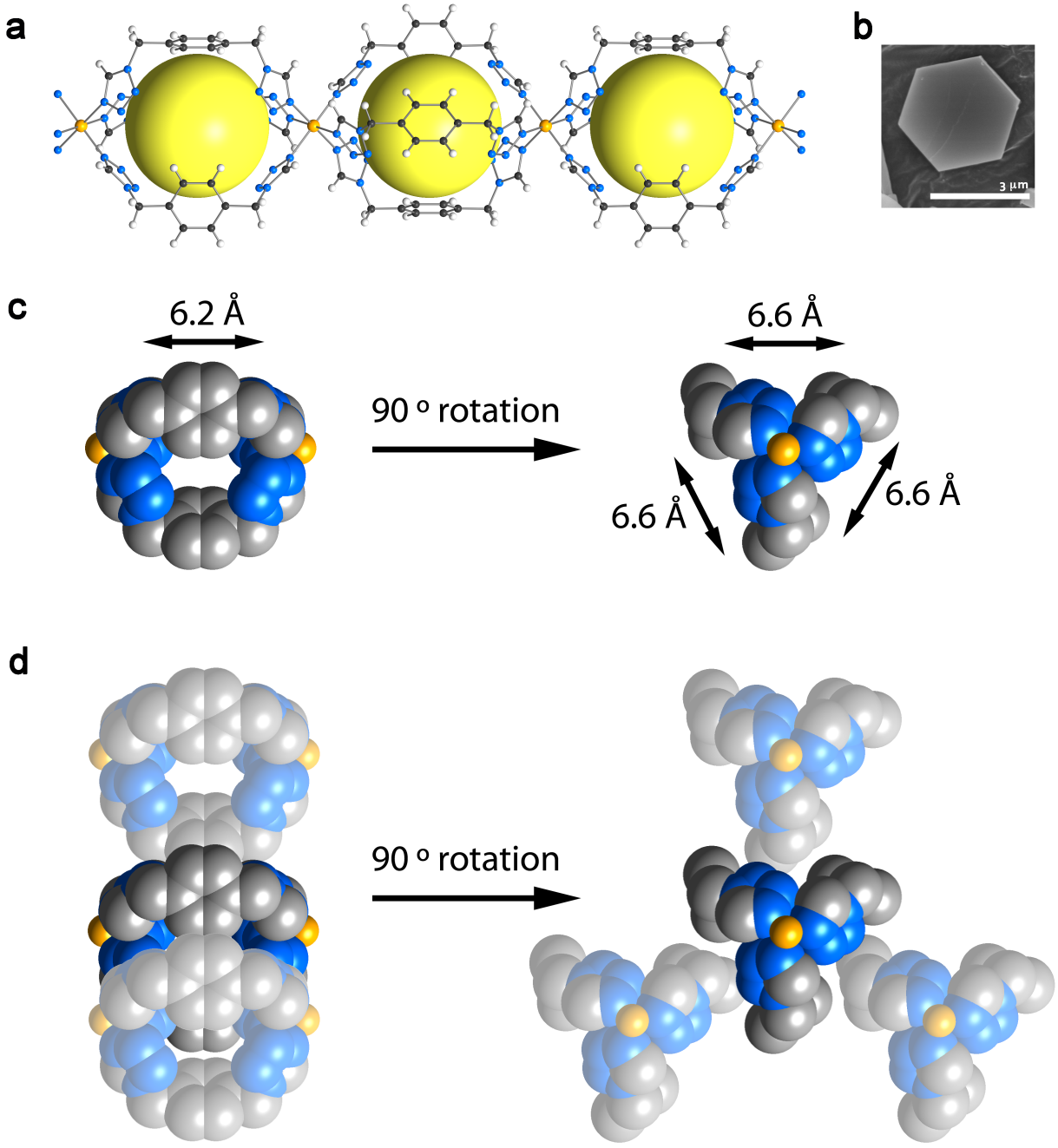

Figure 1. (a) Partial crystal structure of the compartmentalized coordination polymers **CCP-1** and **CCP-2** emphasizing the internal cavities (as yellow spheres) formed by the connection of iron(II) centres to three bistetrazol-*p*-xylene ligands in *syn* conformation. Key: Fe, orange; C, gray; N, blue; H, white; counteranions (ClO_4^- and BF_4^-) omitted for clarity. (b) Scanning electron microscope (SEM) image of a microcrystal of **CCP-1**, showing the hexagonal morphology. (c) Each individual void present windows of dimensions 6.2 x 6.6 $Å^2$. (d) Three adjacent chains cause the blockage of

the three void windows.

Gas sorption: thermodynamic and kinetic study. Single-component gas sorption isotherms serve to determine the loading capacities of **CCP-1** and **CCP-2** towards each different gas in a thermodynamic equilibrium as well as their possible preferentiality to specific gases. Figure 2a shows the total sorption uptake at 298 K for CO_2, CO, N_2, CH_4, ethane (C_2H_6), ethylene (C_2H_4), and acetylene (C_2H_2). It reveals that each void of the structures is able to allocate *circa* a single molecule of CO_2, CH_4, C_2H_4 and C_2H_2; on the contrary, C_2H_6, CO and N_2 behave markedly different and are not as efficiently sorbed, thus suggesting a preferential sorption for certain gases. Quite remarkable, it can be clearly observed from Figure 2a that **CCP-1** can absorb more CO_2 than C_2H_2 at 100 KPa, which is contrary to the common behaviour of most MOFs, that show a preferential adsorption of C_2H_2 over CO_2 under the same condition.[29] The dense nature of compounds **CCP-1** and **CCP-2** resulting from the lack of permanent pores causes a significant volumetric gas storage capacity (e.g. CO_2 capacity of 29 $cm^3 \cdot cm^{-3}$ $vol_{CO_2}/vol_{material}$ and 27 $cm^3 \cdot cm^{-3}$ for **CCP-1** and **CCP-2**, respectively), which is of the same order as other archetypal MOF structures (e.g. 28 $cm^3 \cdot cm^{-3}$ for MIL-100,[30] and 11 $cm^3 \cdot cm^{-3}$ for MOF-5[31]) at the same temperature and pressure (1 bar and 298 K). However, the chemical design of these compartmentalized coordination polymers causes the trapping of the gas molecules in the internal voids without using any specific directional groups, neither covalent bonds (e.g. open metal sites) nor supramolecular interactions (e.g. hydrogen bonding), which are typically introduced in the frameworks and are commonly associated with the strength of the gas interaction with the adsorbent. As a consequence, the isosteric enthalpy of adsorption at zero surface coverage of the different gas molecules in compartmentalized coordination polymers **CCP-1** and **CCP-2** is rather low, regardless of the chemical nature of the gas (Q_{st} (CO_2) = 20 $kJ \cdot mol^{-1}$; Q_{st} (C_2H_2) = 23 $kJ \cdot mol^{-1}$; Q_{st} (CO) = 11 $kJ \cdot mol^{-1}$). This has important implications in the energy cost for regeneration of the material subsequent to saturation and therefore gives a very high working capacity for adsorption-desorption cycles, which is the most significant aspect for gas storage applications, as well as implies that heat management during adsorption-desorption cycles will be easier than using other MOF-based adsorbents. For example, functionalized MOFs with alkylamines show enthalpies of adsorption as high as 96 $kJ \cdot mol^{-1}$ and typically require temperatures in excess of 100 °C to fully regenerate.[32]

Another relevant aspect in the study of selectivity relates to the kinetic sorption due to the dissimilar diffusivity of different gases. Commonly, gas storage studies focus on equilibrium gas adsorption, but adsorption dynamics and diffusion through the structure are important

characteristics that can be exploited for separation processes.[33,34] As a consequence of the lack of permanent channels in compounds **CCP-1** and **CCP-2**, an enhanced kinetic selectivity is developed. In fact, the gas isotherms at different temperatures reveal the presence of diffusion problems in certain gases (Figure S5), which prompted us to examine the transport diffusion of CO_2, CH_4, C_2H_6 and C_2H_4 (note that for chemical compatibility of the thermogravimetric instrument and safety issues, the transport diffusion of C_2H_2 could not be examined, but is expected to be analogous to that of CO_2 as both gases have similar dimensions, polarizabilities and quadrupolar moments, see Table S6). Figure 2b shows the gravimetric evolution upon exposing compound **CCP-1** to 300 mbar of different gases at 298 K. CO_2 is readily adsorbed, a behavior that is also expected for acetylene. On the contrary, sorption of ethylene is more difficult, which is even slower in the case of ethane and methane. This trend could be related with the different molecular dimensions of the gases, the decrease in the quadrupolar moment, the different polarizability, or a combination of these physical properties (see Table S6 for values). Nevertheless, this indicates a possible method to separate mixtures of acetylene/ethylene/light hydrocarbons (methane, ethane, propane) by kinetic trapping.

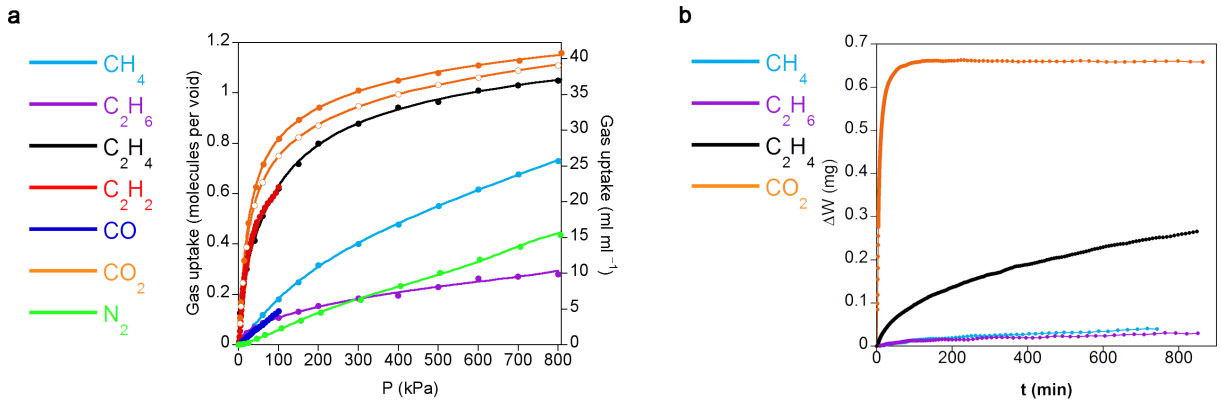

Figure 2. (a) Gas adsorption isotherms at 298 K of **CCP-1** (closed symbols) and **CCP-2** (open symbols) of different gases (lines correspond to the best fits). Data at other temperatures are shown in Supporting Information. (b) Kinetic sorption of **CCP-1** for different hydrocarbons and CO_2, keeping a constant pressure of 300 mbar at 298 K.

Gas sorption: selectivity study. In addition to gas storage with low heat of adsorption, separation and purification processes need high selectivity for specific species. Flexible MOFs working with a "gate opening" process,[35] or pore expansion ("breathing effect"),[36] have shown their importance in selective sorption, as only certain gases can open the pores of the materials. However, once these molecules have opened the path, other undesired species can diffuse into the solid, thus

dramatically diminishing the selectivity as has been previously speculated,[37] and therefore reducing its overall utility for separation. Nevertheless, a recent example combines the gate opening behaviour of the framework with the different electronic properties of gases to accomplish a preferential adsorption of CO_2 over C_2H_2, which is rarely observed.[29]

To have a more precise understanding on the gas separation capacity of these CCPs, we have performed breakthrough experiments under kinetic gas-flow conditions, imitating real situations. Many examples in the literature base their gas selective studies on the analysis of the isolated isotherms or computer simulations using an Ideal Absorbed Solution Theory (IAST). These methods are easier to carry out than performing real gas mixture studies, but in many cases result inaccurate due for instance to difficulties in the kinetic and thermodynamic gas sorption mechanisms, thus obtaining selectivities often far from the real values. Gas mixture adsorption was measured from breakthrough experiments on a column packed with **CCP-1**, previously pelletized to avoid a high-pressure drop over the column. Four different compositions have been analyzed for both CO_2/N_2 and CO_2/CH_4 mixtures, by increasing the CO_2 concentration (5:95, 10:90, 20:80 and 50:50) (Figures S9 and S10). Even though the low kinetics of CO_2 sorption by the system is evident with a gradual release of CO_2 at early stages, **CCP-1** effectively separates CO_2 from N_2 or CH_4 in all cases, with respective experimental selectivities (α) as high as 85 and 89, obtained via mass balance calculations for each different mixture compositions (see Supporting Information). When the separation factor is examined as a function of the feed fraction, it is observed that the best separation capabilities is achieved at low CO_2 concentrations, with both methane and nitrogen as competitors, as has also been previously reported for NH_2-MIL-101(Al).[44] This trend is in agreement with the separation process being controlled by kinetics, as a lower CO_2 flux implies a longer mass transfer in the column. These outstanding separation performances surpass the values reported for other MOFs under similar conditions determined by breakthrough experiments (see Table 1), with the benefit of **CCP-1** being highly selective for two different mixtures, CO_2/N_2 and CO_2/CH_4. More interesting conclusions arise from examination of the adsorbed gas phase through mass spectrometry, which reveals the presence of a highly enriched composition of CO_2 regardless the composition of the injected mixture, demonstrating a significantly higher affinity for CO_2 than for N_2 and CH_4. As shown in Figure 3, the partition coefficient (P) after sorption of different CO_2:N_2 or CO_2:CH_4 mixtures, defined as $P = (X_{CO_2}/Y_{CO_2})/(X_{gas}/Y_{gas})$, have values in the range 30–50, which clearly enhances the performances of other porous solids (see Table 2).

Table 1. Experimental selectivities (α) of selected MOFs obtained *via* mass balance calculations using data from breakthrough experiments.

Compound	Selectivity (α)		Flow composition		Pressure (bar)	Ref.
	CO_2/N_2	CO_2/CH_4	CO_2:N_2	CO_2:CH_4		
CCP-1	85	89	5:95	5:95	2	this work
CCP-1	33	42	10:90	10:90	2	this work
CCP-1	11	15	20:80	20:80	2	this work
CCP-1	2	2	50:50	50:50	2	this work
CTF-1	18	–	10:90	–	1	38
CTF-1-600	21	–	10:90	–	1	38
FCTF-1	77	–	10:90	–	1	38
FCTF-1-600	152	–	10:90	–	1	38
SIFSIX-2-Cu-i	72	51	10:90	50:50	1	39
MOF508b	5	3	50:50	50:50	4 / 1	40
MOF-5	22	–	20:80	–	1	41
NH_2-MIL-53	–	45	–	50:50	1	42
CPO-27-Ni	–	15	–	50:50	1	43
CPO-27-Co	–	12	–	50:50	1	43
CPO-27-Zn	–	9	–	50:50	1	43
STA-12-Ni	–	6	–	50:50	1	43
NH_2-MIL-101 (Al)	–	65	–	15:85	1	44
MIL-53 (Cr)	–	13	–	25:75	1	45
MIL-53 (Al)	–	7	–	30:70	1	46
MIL-101 (Cr)	–	7.5	–	30:70	1	44

Table 2. Experimental selectivities of selected MOFs obtained by experimental determination of adsorbed compositions.

Compound	Partition coefficient (P)		Flow composition		Pressure (bar)	Ref.
	CO_2/N_2	CO_2/CH_4	CO_2:N_2	CO_2:CH_4		
CCP-1	35	47	5:95	5:95	2	this work
CCP-1	38	41	10:90	10:90	2	this work

CCP-1	36	36	20:80	20:80	2	this work
CCP-1	49	32	50:50	50:50	2	this work
Cu-BTC	–	6	–	25:75	1	47
Ni-MOF-74	38	–	15:85	–	1	48
UiO-66(Zr)-$(COOH)_2$	56	–	15:85	–	1	49
CID-3	39	–	1:99	–	30	50

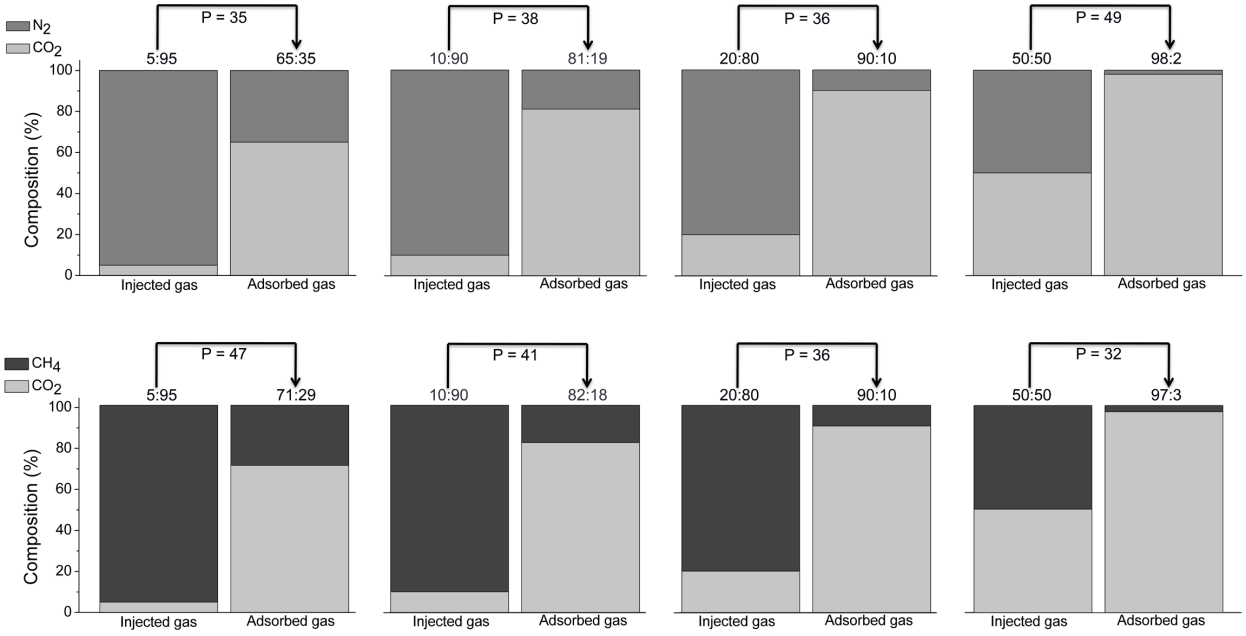

Figure 3. Enrichment of the CO_2 component after gas separation experiments obtained by flowing different mixtures of CO_2/N_2 (top) and CO_2/CH_4 (bottom) at 298 K. Gas compositions determined by gas chromatography.

Location and binding of gas molecules. In order to understand the adsorption process of these compartmentalized coordination polymers, we have combined spectroscopic and diffraction experiments to unveil the interaction of the CO_2 molecules with frameworks **CCP-1** and **CCP-2**. We combine Inelastic Neutron Scattering (INS) and Density Functional Theory (DFT) calculations in order to perform a full description of the experimental spectra. Firstly, we have been able to successfully reproduce the experimental INS spectra of bare **CCP-1** using the aClimax software[51] with the fundamental modes from the DFT calculations (Figure 4a). A description of the analysis of

some fundamental modes can be found in the Supplementary Information. Figure 4b shows the comparison of the INS spectra of bare **CCP-1** and loaded with CO_2 (top) with the H partial density of states, $g_H(\omega)$, obtained from *ab-initio* Molecular Dynamics simulations, showing a good agreement with the experimental spectra. The vibrational spectra of **CCP-1** remains practically unchanged upon CO_2 sorption, with only some differences observed in the intensity of some vibrational bands, but no changes in band positions is observed. Thus, a minor interaction is observed between the sorbed CO_2 molecules and the framework, with a small change in intensities in some vibrational bands. In order to identify the contribution of the different hydrogen atoms of the vibrational spectra, we have analyzed the trajectories of the different H atoms, leading to the partial density of states of the different functional groups, $g_H(\omega)$, $g_{H\text{-phenyl}}(\omega)$, $g_{H\text{-methylene}}(\omega)$ and $g_{H\text{-tetrazole}}(\omega)$, for the total contribution of all the H atoms in the crystal, in the phenyl ring, of the methylene group and of the tetrazole group respectively (Figure S15). It can be seen that the larger changes upon CO_2 sorption comes from the contribution of the methylene and tetrazole groups, although the interaction is rather weak. INS has previously been shown to effectively determine the changes in a hydroxyl group of a MOF caused by CO_2 sorption,[52] thus allowing an indirect observation of the binding mechanism. In that study, Yang, Schröder and co-workers observed two major increases in peak intensity upon CO_2 sorption, which were rationalized by DFT calculations to correspond to changes in the O–H and the aromatic C–H groups caused by interactions with the nucleophilic oxygen atom of the gas molecule. Very differently, we have succeeded to observe the scattering of the adsorbed CO_2 molecules despite their small scattering cross-section. To the best of our knowledge, this is the first time that the neutron vibrational spectrum of adsorbed CO_2 in a MOF has been measured. Specifically, we unambiguously observe an increase in band intensity at 650 cm^{-1} (81 meV) upon CO_2 sorption, which is the only change observed in the 500–800 cm^{-1} region (Figure 4c). This band corresponds to the bending of the CO_2 molecule and, as observed in Figure 4c, can be clearly assigned despite the neutron spectra being mainly dominated by the vibrational bands of the framework.

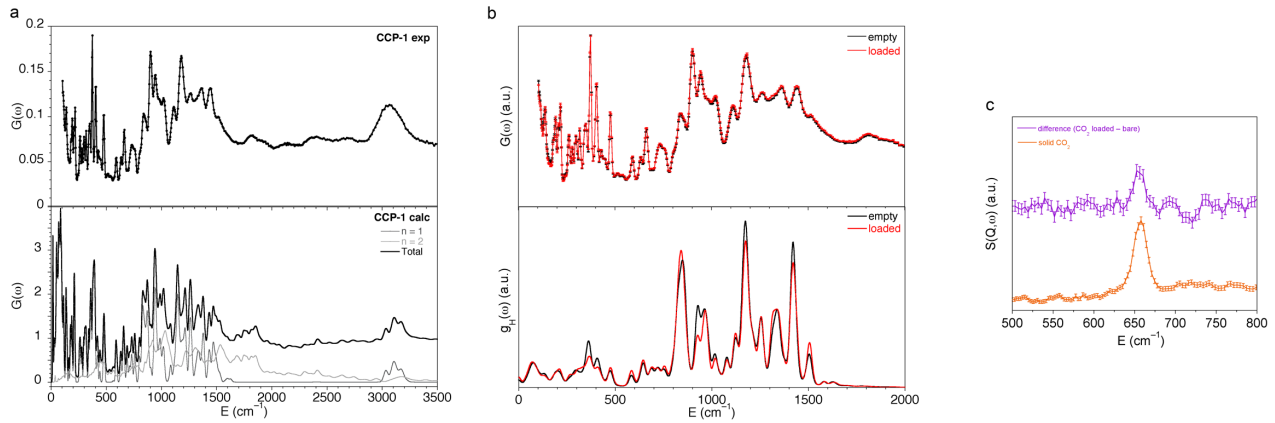

Figure 4. (a) Comparison of the experimental (top) and the calculated (bottom) INS spectra for bare **CCP-1** obtained with the software aClimax[51] including the fundamental frequencies and the first overtones. (b) Comparison of the experimental INS spectra (top) and hydrogen partial density of states, g_H (ω), obtained from *ab-initio* Molecular Dynamics simulations (AIMD) (bottom) for bare **CCP-1** (in black) and **CCP-1** loaded with CO_2 (in red). (c) Difference plot for experimental INS spectra **CCP-1** loaded with CO_2 and bare **CCP-1**, and that of solid CO_2.

Additionally, the presence of ordered cavities in compartmentalized extended systems can structurally control the positioning of gases without the need of directional interactions. As a result, the included guests are regularly located, enabling the crystallographic analysis of the accommodated gases and thus allowing the direct visualization of these molecules inside the cavities. This contrasts with the common situation encountered in porous coordination networks, where guests are severely disordered and are rarely observed by X-ray analysis.[53] Therefore, we have proceeded to the *in situ* structural determination of both **CCP-1** and **CCP-2** under 6 bar of CO_2, ethylene (C_2H_4) and methane (CH_4), using synchrotron X-ray powder diffraction data (Figure 5). Upon activation of the material, no residual electron density is observed within the voids (see Figure S4). The increase of gas pressure produces the appearance of electron density in the internal cavities. This has been analyzed using the Rietveld method, refining the occupancy of the gas molecules(CO_2, C_2H_4 or CH_4) introduced as rigid bodies with a constrained thermal parameter. The counterions (ClO_4^- and BF_4^-) remain in all cases in the same position, not being influenced by the sorption process.

In all cases the gas molecules are disordered over six symmetry related positions, with a total refined occupancy that is close to the calculated loading from the adsorption isotherms (see Table 3). Although all the structures present the gas molecules located inside the internal voids, the gas-framework interaction differs on the three gases. Thus, the CO_2 interacts with the cationic

framework in an end-on mode through the nucleophilic oxygen atom, with a O=C=O(δ–)···π_{N-N} distances of 2.500 Å for **CO_2@CCP-1** and 2.778 Å in **CO_2@CCP-2**. No interaction is found between the framework and the electrophilic carbon atom, possibly due either to the cationic nature of the framework or to the constrained space of the void, or to a combination of both. The C_2H_4 forms C–H···π_{N-N} hydrogen bonds with the frameworks, with C–H···π_{N-N} distances of 2.684 and 2.677 Å for **C_2H_4@CCP-1** and **C_2H_4@CCP-2**, respectively. Finally, the adsorbed CH_4 molecules form C–H···π_{N-N} distances of 2.661 and 2.781 Å for **CH_4@CCP-1** and **CH_4@CCP-2**, respectively.

Table 3. Refined occupancies of gas molecules of gas-loaded structures at 295 K and 6 bar

	CO_2	C_2H_4	CH_4
CCP-1	1.123(7)	0.818(8)	0.78(3)
CCP-2	1.044(10)	0.899(14)	0.84(3)

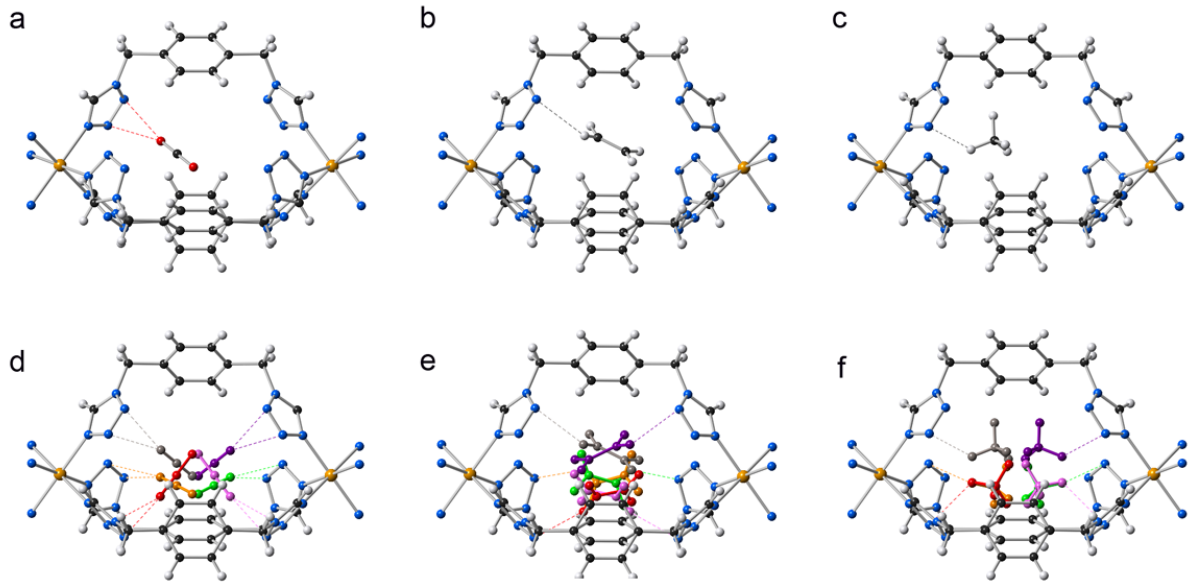

Figure 5. Crystal structures of **CCP-1/CCP-2** loaded with CO_2 (a), C_2H_4 (b) and CH_4 (c), showing the interactions between the gas molecules and the framework as dashed lines. The symmetry-related gas molecules are colored differently showing the positional disorder of the CO_2 (d), C_2H_4 (e) and CH_4 (f) molecules. Anions have been omitted for clarity. Colors of the framework: Fe, orange; C, gray; N, blue; O, red.

Further comprehension of the strength of the gas-framework interaction has been achieved by analyzing the effects of the adsorbed molecules in the magnetic and chromatic thermal–induced spin transition exhibited by **CCP-1** and **CCP-2**. Magnetic susceptibility measurements performed

on polycrystalline powders of **CCP-1** and **CCP-2** show that both compounds unequivocally display a complete spin transition from the high-spin (HS) to the low-spin (LS) state centered at 200 K, which is not affected by the choice of the counteranion. The magnetic response of compounds **CCP-1** and **CCP-2** upon exposure to different gases is presented in Figure 6. Although reversible changes in the transition temperature are uncommon in non-porous spin-crossover materials,[26,27,54-56] these two analogous compounds display similar gas–responsive behavior, which can be related to the gas-framework interaction.

Loading of CO_2 gas molecules onto **CCP-1** and **CCP-2** induces an increase of the $T_{1/2}$ in both systems, i.e. physisorption of CO_2 gas molecules into the cavities of the two frameworks serve to stabilize the LS state (Figures 6a and 6b). This modification in the transition temperature depends on the number of CO_2 molecules incorporated in the framework cavities, which has been proved in a dual manner. A partial loading of pure CO_2 (Figure 6c), or the use of different dilutions with N_2 (Figure 6d) causes in all cases a partial increase that is related only to the amount of CO_2 that is adsorbed. The sorption of a gas with opposed quadrupolar moment to CO_2, e.g. ethylene, causes the opposite response from the framework, i.e. a small reduction in the transition temperature, whereas methane, ethane and CO do not affect the transition temperature (Figure 6e-6i). This provides important information regarding the gas-framework interaction. Whereas the gas-framework interaction is strong and moderate for CO_2 and ethylene, respectively, methane molecules interact very weakly with the framework once inside the voids, despite the gas···framework distance being similar than in the case of ethylene. This can be ascribed to the different quadrupolar moment of the gases, which is in the order CO_2 > C_2H_4 > CH_4 (see Table S6). Remarkably, propane inclusion causes an enhanced cooperativity between the metal centers (i.e. a large increase in the thermal hysteresis), likely mediated by the presence of gas molecules in the voids. Still, the slow diffusion of this gas makes the study of the adsorption isotherm unfeasible.

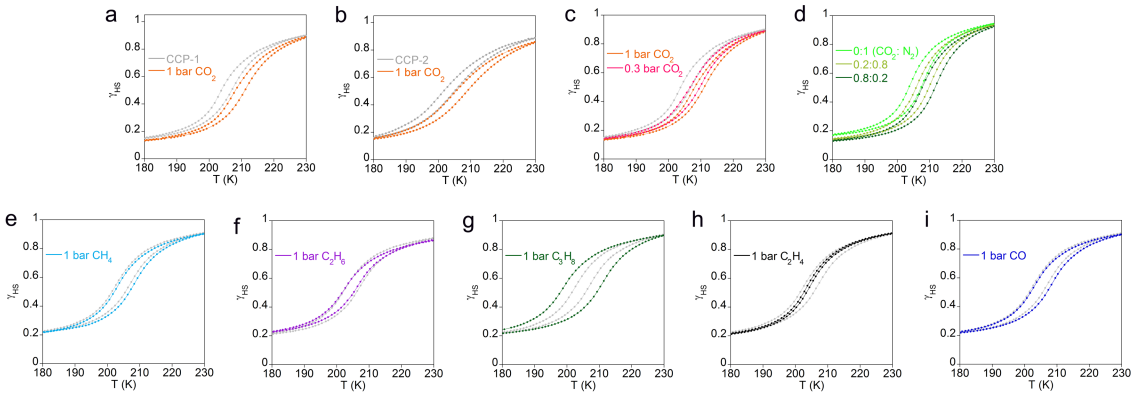

Figure 6. (a,b) Temperature dependence of the high spin fraction (γ_{HS}) for **CCP-1** and **CCP-2** before and after CO_2 inclusion; as-synthesized **CCP-1** and **CCP-2** shown in grey and loaded with 1 bar of CO_2 shown in orange. (c,d) Detailed view of the spin transition region of **CCP-1** upon partial loading of CO_2 and using different dilutions with N_2. (e-i) Detailed view of the spin transition region of **CCP-1** upon loading with different gases: methane, ethane, propane, ethylene and CO. The spin transition of the activated material is shown in grey in each case for comparison.

Diffusion mechanism. Given the lack of permanent channels in compounds **CCP-1** and **CCP-2**, the most plausible mechanism for gas sorption consists in the rotation of the phenyl rings of the btzx ligands, which block the access to the cavity. In order to gain insight on the mechanistic aspects of the gas sorption, we have combined Quasielastic Neutron Scattering (QENS) experiments with Molecular Dynamics simulations. QENS is often used to probe the diffusion dynamics of molecules incorporated in porous materials. However, in this case we have used this technique in a different way, aiming at probing the dynamics in the framework, i.e. the change in orientation of the aromatic rings, which would be at the origin of the mechanism of diffusion. QENS is highly sensitive to the movement of hydrogen atoms and, therefore, perfectly suited to probe the existence of rotating aromatic rings,[57] especially given the tiny cross section of C and O. Upon sorption of the gas, the presence of the CO_2 molecules is expected to interfere with the rotation of the phenyl rings, causing a clear change of the QENS signal. However, the experimental data do not show significant changes upon sorption. The presence of the gas in the compartments is evidenced by the decrease in intensity of some of the Bragg peaks due to the reduction in contrast with respect to the framework (Figure S17). Furthermore, some minor additional intensity in the range ±0.5 meV can also be detected, and could be related to a fast diffusion of CO_2 into the solid. However, as the scattering contribution from CO_2 represents at best only 0.5 % of the total scattering signal, no clear conclusions can be obtained based solely on these data (Figure 7a). In the same way, the elastic incoherent structure factor (EISF), which can be used as a measure of the delocalization of the scatterers,[58] remains practically unchanged upon CO_2 sorption and indicates the absence of appreciable rotational motion of the phenyl rings in both the bare and loaded systems (Figure S16). These counterintuitive results have been unveiled by atomistic molecular dynamics techniques. Using a modified version of the Universal Force Field,[59] we have been able to describe the dynamics of CO_2 penetration in the internal cavities. Thus, when the compartmentalized coordination polymer is completely empty and a low CO_2 pressure is applied, gas molecules start to fill the voids. Then, an increase of pressure causes the eventual presence of two CO_2 molecules in the same cavity, which augments the energy of the system, thus producing a migration of one of

these molecules to an adjacent empty void (see Figure 7b and Supporting Movie 1). Molecular dynamics calculations show that this movement of migration of CO_2 molecules from one cavity to another is very slow, and can be explained by a gate opening mechanism of the phenyl rings (Figure 7c), which only takes place to allow the transition of the gas molecules. Therefore, although this fast movement lies within the time scale of QENS, only some phenyl rings rotate at any specific moment, the vast majority of the rings remaining static. Thus, the probability of experimentally detecting the movement of the phenyl ring during the process of migration is minute, which is in agreement with the observations of QENS.

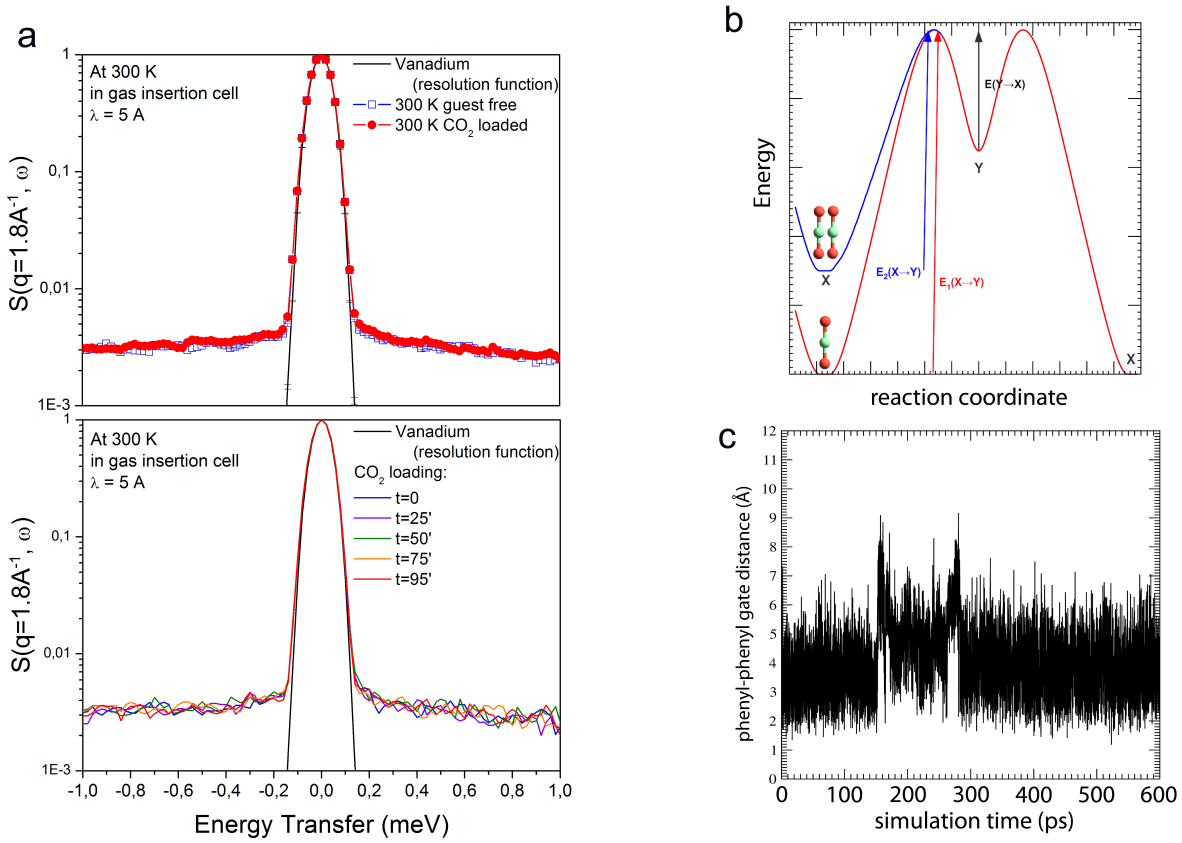

Figure 7. (a) QENS spectra for bare **CCP-1** and **CCP-1** loaded with CO_2 at 300 K (top) and in-situ measurement during CO_2 loading (bottom). (b) Energetic scheme corresponding to the diffusion of CO_2 through **CCP-1**. 'X' is the cavity corresponding to the minimum energy and 'Y' is a higher energy location. When two CO_2 molecules fill the 'X' cavity, their energy in the cavity increases, activating the diffusion. (c) Interphenyl distance showing the gate opening mechanism in **CCP-1** during the 600-ps molecular dynamics calculation where the intercavity transition of a CO_2 molecule can be observed. The H–H distance corresponds to atoms of adjacent chains, which have been selected according to the scheme in Figure S22. The times at which the two steps of the

intercavity migration occurs are clearly observed at ca. 150 and 275 ps, and correspond to the transitions X → Y and Y → X of Figure 7b. The total duration of the migration can be estimated in ca. 135 ps.

CONCLUSIONS

The presence of discrete compartments interconnected by dynamic apertures has a strong influence for the discrimination of very similar species, which relies in the different possible mechanisms towards selective sorption. These are based either on thermodynamic equilibrium or kinetic conditions, both of which have been examined with the use of an ample range of experimental techniques complemented by theoretical calculations. This multi-technique analysis has revealed that the peculiar structural arrangement found in **CCP-1** and **CCP-2** results not only in an extremely high selective sorption of CO_2 in the presence of N_2 or CH_4, as experimentally shown by breakthrough experiments with α and P values as high as 89 and 49, respectively, but also in the possibility of kinetic separation of ethane/ethylene/acetylene. Synchrotron powder X-ray diffraction has been used to unveil the location of the gas molecules (CO_2, CH_4 and C_2H_4) in the interior of the pores and their binding modes with the framework. Taking advantage of the magnetic properties of **CCP-1** and **CCP-2**, which present spin-crossover phenomena, the strength of the interaction between the gas molecules and the framework has been elucidated through the effects exerted in the transition temperature. The strongest response has been found for CO_2, which has been evaluated in detail with inelastic neutron scattering and quasi-elastic neutron scattering, revealing the mechanism of entrance of these molecules. Additionally, molecular dynamics simulations have served to rationalize the experimental findings. A fast movement of the benzyl rings allows the passing of the CO_2 molecules from void to void via a transition state that is located in the intervoid region.

The present results pave the way for the design of further compartmentalized coordination polymers with enhanced sorption capabilities while maintaining the high selectivity demonstrated by **CCP-1** and **CCP-2**. Typically, MOFs materials possess either thermodynamic selective sorption or kinetic selectivity, while the coordination polymer here presented represents a unique example showing both types of selectivity. Additionally, this approach permits the isolation of specific molecules within a confined space, thus allowing a detailed study of individual molecules in the absence of self-interactions. This situation is similar to that encountered in the encapsulation of small molecules in fullerene cages.[60] Still, compartmentalized coordination polymers offer the

advantage that the size of these compartments can be tuned and larger species can therefore be encapsulated.

ACKNOWLEDGEMENTS

Financial support from the Spanish MINECO (CTQ2014-59209-P and MAT2014-56143-R), the Generalitat Valenciana (Prometeo and ISIC-Nano programs), the EU (ERC-2016-CoG 724681-S-CAGE) and the VLC/Campus Program is gratefully acknowledged. We thank the Spanish government for the provision of a Severo Ochoa project (SEV-2012-0267) and a María de Maeztu project (MDM-2015-0538). M.G.-M. thanks MICINN for a predoctoral FPU grant and the EU for a Marie Sklodowska-Curie postdoctoral fellowship (H2020-MSCA-IF-EF-658224). N.C.G. thanks the Generalitat Valenciana for a VALi+d predoctoral fellowship. J.A.R.-V. acknowledges CSIC for a JAE-doc contract. G.S. thanks SGAI-CSIC for computing time. G.M.E. acknowledges the Blaise Pascal International Chair for financial support and the Ramón y Cajal Programme. J. M. Martínez-Agudo and G. Agustí from the University of Valencia are gratefully acknowledged for magnetic measurements. We are grateful to Institut Laue-Langevin for neutron beam time allocation for INS and QENS experiments (doi:10.5291/ILL-DATA.7-05-426). Authors thank ALBA Synchrotron for beamtime allocation at BL04-MSPD beamline for HR-PXDR measurements, as well as the collaboration of ALBA staff during the experiment (proposal 2015091491).

EXPERIMENTAL

Synthesis. CCP-1 and **CCP-2** were prepared in high yields as single-phase crystalline materials adapting a previously described methodology.[26] Alternative synthesis using microwaves has been successfully applied (see Supporting Information).

Crystal data for CCP-2. $[Fe(C_{10}H_{10}N_8)_3](BF_4)_2$. Colorless hexagonal plate. Space group $P6_3/m$, Z = 2, M = 956.25. **HS**: T = 240(2) K, $a = b$ = 10.4852(10) Å, c = 23.308(3) Å, V = 2219.2(5) Å^3. R1 = 0.1085 and wR2 = 0.3038. **LS**: T = 120(2) K, $a = b$ = 10.3690(5) Å, c = 22.9628(15) Å, V = 2138.1(2) Å^3. R1 = 0.1090 and wR2 = 0.2978.

Crystal data for gas loaded materials. Data was collected on beamline BL04-MSPD at ALBA Synchrotron, Spain, using λ = 0.799332 Å and a Mythen detector comprising 6 modules. The samples were pumped for ca. 30 minutes, after which the gas pressure was increased to 6 bar. The capillaries were allowed for 30-minute stabilization before data collection at 295 K. The final Rietveld plots correspond to satisfactory crystal structure models converging to R_{wp} = 0.0214, gof = 2.183 in **CO_2@CCP-1**, R_{wp} = 0.0162, gof = 1.919 in **C_2H_4@CCP-1**, R_{wp} = 0.0107, gof = 1.285 in

CH_4@CCP-1, R_{wp} = 0.0313, gof = 3.271 in **CO_2@CCP-2**, R_{wp} = 0.0357, gof = 3.738 in **C_2H_4@CCP-2**, and R_{wp} = 0.0329, gof = 3.442 in **CH_4@CCP-2**. Details on the refinement are given in the Supporting Information.

Gas sorption. High-resolution isotherms were measured at a series of temperatures in a Micromeritics ASAP 2010 volumetric instrument using approximately 150 mg of sample as a powder. Prior to adsorption experiments, the sample was outgassed at 423 K for 6 hours under turbomolecular high vacuum. High-pressure adsorption isotherms and kinetic measurements were performed in an IGA-3 gravimetric analyser (Hiden Isochema). Approximately, 50 mg of sample were placed in the balance. Before each adsorption experiment, the sample was outgassed at 423 K under a final pressure of 10^{-5} Pa during four hours. Breakthrough experiments were performed in a home-made instrument (details in Supporting Information) using 1.2375 g of sample previously pelletized. Prior to the breakthrough experiments, the adsorbent was activated at 353 K in 40 ml/min of helium for two hours.

Magnetic measurements. Magnetic susceptibility measurements were carried out with a Quantum Design MPMS-XL-5 SQUID susceptometer. The susceptibility data were all collected at 1 K·min^{-1}, with an applied field of 0.1 T. Measurements of the gas loaded systems were performed by sealing a glass tube with 10 mg of **CCP-1** and **CCP-2** and a known amount of the gas (CO_2, CH_4, C_2H_6, C_2H_4, CO, propane, N_2, N_2/CO_2) or after heating a loaded sample to remove the CO_2 molecules.

Inelastic neutron scattering. The INS spectra were measured at 5 K in the range of energy transfers from 16 to 4000 cm^{-1} with and energy resolution of $\Delta E/E \approx 2$ using LAGRANGE, the neutron vibrational spectrometer installed at the hot source of the high-flux reactor at the Institute Laue-Langevin (ILL, Grenoble, France). The background spectrum from the cryostat and an empty sample holder was measured separately and then subtracted from the raw INS spectrum of the sample. Data sets were then normalized for monitor counts and corrected for empty cell. The sample was placed in an Al cell connected to the gas injection stick. The aluminum cell was placed inside a cryostat allowing a precise temperature control.

DFT calculations. The theoretical vibrational spectra were calculated using the direct method on the basis of first-principles calculations. Calculations of the relaxed structure of a unit cell consisting in 200 atoms and the eigen modes, obtained from the dynamical matrix, were calculated by using the DMol3 ab initio simulation package in Materials Studio software package.[61] The electron exchange and correlation are treated within the generalized gradient approximation (GGA) in the Perdew-Burke-Ernzerhof (PBE) form.[62] Experimental lattice parameters were fixed in the calculation to the experimental ones and only the atomic positions were relaxed. All electronic functions were calculated at the Γ- point.

The vibrational spectra is calculated from the partial density of states, $g_i(\omega)$, of the different atomic species: $VDOS(\omega) \approx \sum_i g_i(\omega)$. In the case of this study, due to the predominant ratio σ_H/M_H of hydrogen, the measured spectrum is essentially $g_H(\omega)$, the partial vibrational density of states (p-VDOS) of H.

Quasielastic neutron scattering. The QENS experiments were performed in the direct time-of-flight spectrometer IN5 at the Institut Laue-Langevin (ILL, Grenoble, France). Two incident neutron wavelengths were used: 5 Å (3.27 meV), yielding an energy resolution (full-width at half-maximum) of 0.1 meV at zero energy transfer and a Q-range of 0.2–2.2 $Å^{-1}$, and 8 Å (1.28 meV) resulting in a resolution of 0.25 meV and a Q-range of 0.2–1.4 $Å^{-1}$. The sample was placed inside a cylindrical aluminium sample holder allowing the gas injection, and temperature control was achieved using a standard ILL Orange cryostat. The empty sample holder was measured in the same conditions and the spectrum subtracted from that of the sample. The detector efficiency correction was performed using data collected from a standard vanadium sample, which is an elastic incoherent scatterer. Basic corrections and data reduction was performed using LAMP software.[63] The data were rebinned at constant Q values. Since for QENS analysis we are only interested in incoherent scattering, all spectra that have contributions from coherent scattering such as Bragg peaks were excluded. The scattering function, $S(Q,\omega)$, spectra were fitted to the sum of a delta-function and a Lorentzian peak, both convoluted with the resolution function (estimated by the measurement of a Vanadium sample), in order to obtain an estimation of the Elastic Incoherent Structure Factor (EISF).

Molecular dynamics calculations. Molecular dynamics were performed using a modified version of the widely used Universal force field (UFF),[64] including a specific parameterization aimed to obtain accurate dispersion interactions to describe better the intermolecular interactions, namely between different parts of the **CCP-1** as well as between the adsorbate (CO_2) and **CCP-1**. The GULP software (version 4.3.2)[65,66] has been used to run the molecular dynamics within the NVT ensemble and a timestep of 1 fs. The simulations comprised two CO_2 molecules and run for 600 ps at 498 K.

REFERENCES

1. Keller, G. E.; Marcinkowsky, A.E.; Verma, S. K.; Williamson, K. D., in Separation and Purification Technology, N. N. Li, J. M. Calo, Eds., Marcel Dekker, New York (1992).
2. Morris, R. E.; Wheatley, P. S. *Angew. Chem. Int. Ed.* **2008**, *47*, 4966–4981.
3. Decoste, J. B.; Peterson, G. W. *Chem. Rev.* **2014**, *114*, 5695–5727.
4. Li, J.-R.; Sculley, J.; Zhou, H.-C. *Chem. Rev.* **2012**, *112*, 869–932.

5. McDonald, T. M.; Mason, J. A.; Kong, X.; Bloch, E. D.; Gygi, D.; Dani, A.; Crocellà, V.; Giordanino, F.; Odoh, S. O.; Drisdell, W. S.; Vlaisavljevich, B.; Dzubak, A. L.; Poloni, R.; Schnell, S. K.; Planas, N.; Lee, K.; Pascal, T.; Wan, L. F.; Prendergast, D.; Neaton, J. B.; Smit, B.; Kortright, J. B.; Gagliardi, L.; Bordiga, S.; Reimer, J. A.; Long, J. R. *Nature* **2015**, *519*, 303–308.
6. Xue, D.-X.; Belmabkhout, Y.; Shekhah, O.; Jiang, H.; Adil, K.; Cairns, A. J.; Eddaoudi, M. *J. Am. Chem. Soc.* **2015**, *137*, 5034–5040.
7. Xiang, S.-C.; Zhang, Z.; Zhao, C.-G.; Hong, K.; Zhao, X.; Ding, D.-R.; Xie, M.-H.; Wu, C.-D.; Das, M. C.; Gill, R.; Thomas, K. M.; Chen, B. *Nature Commun.* **2011**, *2*, 204.
8. Nugent, P.; Belmabkhout, Y.; Burd, S. D.; Cairns, A. J.; Luebke, R.; Forrest, K.; Pham, T.; Ma, S.; Space, B.; Wojtas, L.; Eddaoudi, M.; Zaworotko, M. J. *Nature* **2013**, 495, 80–84.
9. Yang, S.; Lin, X.; Lewis, W.; Suyetin, M.; Bichoutskaia, E.; Parker, J. E.; Tang, C. C.; Allan, D. R.; Rizkallah, P. J.; Hubberstey, P.; Champness, N. R.; Thomas, K. M.; Blake, A. J.; Schröder, M. *Nature Mat.* **2012**, *11*, 710–716.
10. Southon, P. D.; Liu, L.; Fellows, E. A.; Price, D. J.; Halder, G. J.; Chapman, K. W.; Moubaraki, B.; Murray, K. S.; Létard, J.-F.; Kepert, C. J. *J. Am. Chem. Soc.* **2009**, *131*, 10998–11009.
11. Lu, W.; Wei, Z.; Gu, Z.-Y.; Liu, T.-F.; Park, J.; Park, J.; Tian, J.; Zhang, M.; Zhang, Q.; Gentle III, T.; Bosch, M.; Zhou, H.-C. *Chem. Soc. Rev.* **2014**, *43*, 5561–5593.
12. Couck, S.; Denayer, J. F. M.; Baron, G. V.; Rémy, T.; Gascon, J.; Kapteijn, F. *J. Am. Chem. Soc.* **2009**, *131*, 6326–6327.
13. An, J.; Rosi, N. L. *J. Am. Chem. Soc.* **2010**, *132*, 5578–5579.
14. Yang, S.; Lin, X.; Blake, A. J.; Walker, G. S.; Hubberstey, P.; Champness, N. R.; Schröder, M. *Nature Chem.* **2009**, *1*, 487–493.
15. Bloch, E. D.; Queen, W. L.; Krishna, R.; Zadrozny, J. M.; Brown, C. M.; Long, J. R. *Science* **2012**, *335*, 1606–1610.
16. Caskey, S. R.; Wong-Foy, A. G.; Matzger, A. J. *J. Am. Chem. Soc.* **2008**, *130*, 10870−10871.
17. Bae, Y.-S.; Lee, C. Y.; Kim, K. C.; Farha, O. K.; Nickias, P.; Hupp, J. T.; Nguyen, S. T.; Snurr, R. Q. *Angew. Chem. Int. Ed.* **2012**, *51*, 1857–1860.
18. Quartapelle Procopio, E.; Fukushima, T.; Barea, E.; Navarro, J A. R.; Horike, S.; Kitagawa, S. *Chem. Eur. J.* **2012**, *18*, 13117–13125.
19. Fracaroli, A. M.; Furukawa, H.; Suzuki, M.; Dodd, M.; Okajima, S.; Gándara, F.; Reimer, J. A.; Yaghi, O. M. *J. Am. Chem. Soc.* **2014**, *136*, 8863−8866.
20. An, J.; Geib, S. J.; Rosi, N. L. *J. Am. Chem. Soc.* **2009**, *132*, 38−39.

21. Yang, S.; Ramirez-Cuesta, A. J.; Newby, R.; Garcia-Sakai, V.; Manuel, P.; Callear, S. K.; Campbell, S. I.; Tang, C. C.; Schröder, M. *Nature Chem*. **2015**, *7*, 121–129.
22. Xiang, S.; He, Y.; Zhang, Z.; Wu, H.; Zhou, W.; Krishna, R.; Chen, B. *Nature Commun.* **2012**, *3*, 954.
23. Inokuma, Y.; Yoshioka, S.; Ariyoshi, J.; Arai, T.; Hitora, Y.; Takada, K.; Matsunaga, S.; Rissanen, K.; Fujita, M. *Nature* **2013**, *495*, 461–467.
24. Coronado, E.; Giménez-Marqués, M.; Mínguez Espallargas, G.; Brammer, L. *Nature Commun.* **2012**, *3*, 828.
25. Halcrow M. (eds.) Spin-crossover materials properties and applications. Wiley (2013).
26. Coronado, E.; Giménez-Marqués, M.; Mínguez Espallargas, G.; Rey, F.; Vitórica-Yrezábal, I. J. *J. Am. Chem. Soc*. **2013**, *135*, 15986−15989.
27. Calvo Galve, N.; Giménez-Marqués, M.; Palomino, M.; Valencia, S.; Rey, F.; Mínguez Espallargas, G.; Coronado, E. *Inorg. Chem. Front.* **2016**, *3*, 808–813.
28. Spek, A. L. *J. Appl. Cryst.* **2003**, *36*, 7–13.
29. Foo, M. L.; Matsuda, R.; Hijikata, Y.; Krishna, R.; Sato, H.; Horike, S.; Hori, A.; Duan, J.; Sato, Y.; Kubota, Y.; Takata, M.; Kitagawa, S. *J. Am. Chem. Soc*. **2016**, *138***,** 3022–3030.
30. Mason, J. A.; McDonald, T. M.; Bae, T.-H.; Bachman, J. E.; Sumida, K; Dutton, J. J.; Kaye, S. S.; Long, J. R. *J. Am. Chem. Soc*. **2015**, *137*, 4787–4803.
31. Yazaydin, A. O.; Snurr, R. Q.; Park, T.-H.; Koh, K.; Liu, J.; LeVan, M. D.; Benin, A. I.; Jakubczak, P.; Lanuza, M.; Galloway, D. B.; Low, J. L.; Willis, R. R. *J. Am. Chem. Soc*. **2009**, *131*, 18198–18199.
32. McDonald, T. M.; D'Alessandro, D. M.; Krishna, R.; Long, J. R. *Chem. Sci*. **2011**, *2*, 2022–2028.
33. Herm, Z. R.; Wiers, B. M.; Mason, J. A.; van Baten, J. M.; Hudson, M. R.; Zajdel, P.; Brown, C. M.; Masciocchi, N.; Krishna, R.; Long, J. R. *Science*, **2013**, *340*, 960–964.
34. Krishna, R. *Chem. Soc. Rev*. **2012**, *41*, 3099–3118.
35. Horike, S.; Shimomura, S.; Kitagawa, S. *Nat. Chem*. **2009**, *1*, 695–704.
36. Ferey, G.; Serre, C. *Chem. Soc. Rev*. **2009**, *38*, 1380–1399.
37. D'Alesandro, D. M.; Smit, B.; Long, J. R. *Angew. Chem. Int. Ed.* **2010**, *49*, 6058–6082.
38. Zhao, Y.; Yao, K. X.; Teng, B.; Zhang, T.; Han, Y. *Energy Environ. Sci*. **2013**, *6***,** 3684–3692.
39. Nugent, P.; Belmabkhout, Y.; Burd, S. D.; Cairns, A. J.; Luebke, R.; Forrest, K.; Pham, T.; Ma, S.; Space, B.; Wojtas, L.; Eddaoudi, M.; Zaworotko, M. J. *Nature* **2013**, *495*, 80–84.
40. Bastin, L.; Bárcia, P. S.; Hurtado, E. J.; Silva, J. A. C.; Rodrigues, A. E.; Chen, B. *J. Phys. Chem. C* **2008**, *112*, 1575–1581.

41. Jiang, N.; Deng, Z.; Liu, S.; Tang, C.; Wang, G. *Korean J. Chem. Eng.* **2016**, 33, 2747–2755.
42. Couck, S.; Gobechiya, E.; Kirschhock, C. E. A.; Serra-Crespo, P.; Juan-Alcañiz, J.; Martinez Joaristi, A.; Stavitski, E.; Gascon, J.; Kapteijn, F.; Baron, G. V.; Denayer, J. F. M. *ChemSusChem* **2012**, *5*, 740–750.
43. García, E. J.; Mowat, J. P. S.; Wright, P. A.; Pérez-Pellitero, J.; Jallut, C.; Pirngruber, G. D. *J. Phys. Chem C* **2012**, *116*, 26636–26648.
44. Serra-Crespo, P.; Ramos-Fernandez, E. V.; Gascon, J.; Kapteijn, F. *Chem. Mater.* **2011**, *23*, 2565–2572.
45. Hamon, L.; Llewellyn, P. L.; Devic, T.; Ghoufi, A.; Clet, G.; Guillerm, V.; Pirngruber, G. D.; Maurin, G.; Serre, C.; Driver, G.; van Beek, W.; Jolimaître, E.; Vimont, A.; Daturi, M.; Férey, G. *J. Am. Chem. Soc.* **2009**, *131*, 17490–17499.
46. Finsy, V.; Ma, L.; Alaerts, L.; De Vos, D.E.; Baron, G. V.; Denayer, J. F. M. *Micropor. Mesopor. Mater.* **2009**, *120***,** 221–227.
47. Hamon, L.; Jolimaître, E.; Pirngruber, G. D. *Ind. Eng. Chem. Res.* **2010**, *49***,** 7497–7503.
48. Liu, J.; Tian, J.; Thallapally, P. K.; McGrail, B. P. *J. Phys. Chem. C* **2012**, *116*, 9575–9581.
49. Yang, Q.; Vaesen, S.; Ragon, F.; Wiersum, A. D.; Wu, D.; Lago, A.; Devic, T.; Martineau, C.; Taulelle, F.; Llewellyn, P. L.; Jobic, H.; Zhong, C.; Serre, C.; De Weireld, G.; Maurin, G. *Angew. Chem. Int. Ed.* **2013**, *52*, 10316–10320.
50. Nakagawa, K.; Tanaka, D.; Horike, S.; Shimomura, S.; Higuchi, M.; Kitagawa, S. *Chem. Commun.* **2010**, *46*, 4258–4260.
51. Ramirez-Cuesta, A. J. *Comp. Phys. Comm.* **2004**, *157*, 226–238.
52. Yang, S.; Sun, J.; Ramirez-Cuesta, A. J.; Callear, S. K.; David, W. I. F.; Anderson, D. P.; Newby, R.; Blake, A. J.; Parker, J. E.; Tang, C. C.; Schröder, M. *Nature Chem.* **2012**, *4*, 887–894.
53. Carrington, E. J.; Vitórica-Yrezábal, I. J.; Brammer, L. *Acta Cryst. Sect. B* **2014**, *70*, 404–422.
54. Miller, R. G.; Brooker, S. *Chem. Sci.* **2016**, *7*, 2501–2505.
55. Rodríguez-Jiménez, S.; Feltham, H. L. C.; Brooker, S. *Angew. Chem. Int. Ed.* **2016**, *55*, 15067–15071.
56. Costa, J. S.; Rodríguez-Jiménez, S.; Craig, G. A.; Barth, B.; Beavers, C. M.; Teat, S. J.; Aromí, G. *J. Am. Chem. Soc.* **2014**, *136***,** 3869–3874.
57. Rodríguez-Velamazán, J. A.; González, M. A.; Real, J. A.; Castro, M.; Muñoz, M. C.; Gaspar, A. B.; Ohtani, R.; Ohba, M.; Yoneda, K.; Hijikata, Y.; Yanai, N.; Mizuno, M.; Ando, H.; Kitagawa, S. *J. Am. Chem. Soc.* **2012**, *134*, 5083–5089.
58. Bée, M. *Physica B* **1992**, *182*, 323–336.

59. Sastre, G.; van den Bergh, J.; Kapeijn, F.; Denysenko, D.; Volkmer, D. *Dalton Trans.* **2014**, *43*, 9612–9619.
60. Popov, A. A.; Yang, S.; Dunsch, L. *Chem. Rev*. **2013**, *113*, 5989–6113.
61. Materials Studio: http://accelrys.com/products/collaborative-science/biovia-materials-studio/
62. Perdew J. P.; Ernerhof M.; Burke K. *J. Chem. Phys.* **1996**, *105*, 9982–9985.
63. LAMP, the Large Array Manipulation Program. http://www.ill.fr/data_treat/lamp/lamp.html
64. Rappe, A. K.; Casewit, C. J.; Colwell, K. S.; Goddard W. A.; Skiff, W. M. *J. Am. Chem. Soc*. **1992**, *114*, 10024–10035.
65. Gale, J. D. *J. Chem. Soc. Faraday Trans*. **1997**, *93*, 629–637.
66. Gale, J. D.; Rohl, A. L. *Mol. Simul*. **2003**, *29*, 291–341.

AUTHOR CONTRIBUTIONS

M.G.-M. and N.C.G. synthesized the materials. M.G.-M. and G.M.E. contributed to solution and refinement of the structures from single crystal data; M.P., S.V. and F.R. carried out measurements and analysis of adsorption isotherms; G.S. performed the molecular dynamics calculations; I.J.V.-Y., J.L.J., N.C.G. and G.M.E. collected the synchrotron X-ray powder diffraction data; I.J.V.-Y. and G.M.E. analyzed the powder diffraction data; M.J.-R. conducted the inelastic neutron experiments, with contributions from J.A.R.-V., F.R., G.S. and G.M.E.; J.A.R.-V. and M.A.G. performed the quasielastic neutron experiments, with contributions from G.M.E.; M.G.-M, N.C.G, E.C. and G.M.E. analyzed the magnetic data; G.M.E. conceived the research and prepared the manuscript; all authors made comments on the manuscript.

ADDITIONAL INFORMATION

Accession codes: The X-ray crystallographic coordinates for structure reported in this Article have been deposited at the Cambridge Crystallographic Data Centre (CCDC), under deposition numbers CCDC-1439096 (**CCP-2–HS**), -1439097 (**CCP-2–LS**), CCDC-1473649 (**CO_2@CCP-1**), -1473650 (**C_2H_4@CCP-1**), -1473651 (**CH_4@CCP-1**), -1473652 (**CO_2@CCP-2**), -1473653 (**C_2H_4@CCP-2**) and -1473654 (**CH_4@CCP-2**). These data can be obtained free of charge from The Cambridge Crystallographic Data Centre via www.ccdc.cam.ac.uk/data_request/cif.

Table of contents